

Prospects for observing the magnetorotational instability in the Plasma Couette Experiment

K. FLANAGAN¹†, M. CLARK, C. COLLINS, C. COOPER,
I. V. KHALZOV, J. WALLACE AND C. B. FOREST

¹Department of Physics, University of Wisconsin, Madison, WI 53703, USA

(Received ?; revised ?; accepted ?. - To be entered by editorial office)

Many astrophysical disks, such as protoplanetary disks, are in a regime where non-ideal, plasma-specific MHD effects can significantly influence the behavior of the magnetorotational instability (MRI). The possibility of studying these effects in the Plasma Couette Experiment (PCX) is discussed. An incompressible, dissipative global stability analysis is developed to include plasma-specific two-fluid effects and neutral collisions, which are inherently absent in analyses of Taylor-Couette flows in liquid metal experiments. It is shown that at current PCX parameters, the ion-neutral drag significantly affects the azimuthal velocity profile, thus limiting the flows to MRI stable regime. Electrically driven flow (EDF) is proposed as an alternative in which the MRI can destabilize at more easily achievable plasma parameters. Scenarios for reaching MRI relevant parameter space and necessary hardware upgrades are described.

1. Introduction

The magnetorotational instability (MRI), first derived by Velikhov (1959) and Chandrasekhar (1960), has been studied extensively as a possible mechanism of enhanced angular momentum transport in accretion disks (Balbus & Hawley 1991, 1998). In an idealized form, this instability occurs when conducting fluid in a spinning disk is threaded by a weak magnetic field. In order to excite the instability, the fluid must have an angular velocity profile which is decreasing with radius, $\partial\Omega^2/\partial\ln r < 0$, and the magnetic field must be sufficiently weak as to not stabilize perturbations, $(\mathbf{k} \cdot \mathbf{V}_A)^2 < -\partial\Omega^2/\partial\ln r$. In some plasmas, such as weakly-ionized and sparse protoplanetary disks, these ideal MHD conditions may not fully describe the onset of MRI, nor the dynamics in the fully saturated state of MRI-driven turbulence. For example, the two-fluid Hall effect can become important when ions become decoupled from the magnetic field. Consequently, MRI growth only occurs when the magnetic field is antiparallel to the rotation axis (Wardle 1999; Balbus & Terquem 2001).

In nature, the ratio of viscosity and resistivity, a property described by the magnetic Prandtl number, $Pm = \mu_0\sigma\nu$, can vary by many orders of magnitude: $Pm \lesssim 10^{-5}$ in disks around young stellar objects while $Pm \gtrsim 10^5$ around active galactic nuclei. Shearing box simulations have shown that varying $Pm = 0.06 - 4$ can cause the magnitude of the MRI driven turbulent radial momentum transport to vary by two orders of magnitude (Longaretti & Lesur 2010), suggesting that the MRI may not be efficient at small Prandtl numbers.

While direct numerical simulations of accretion disks are prohibitive, a laboratory

† Email address for correspondence: ksflanagan@wisc.edu

plasma could create the MRI with $Pm \sim 1$, in which case simulation can resolve all of the critical scales in the parameter range of the experiment, possibly leading to an understanding of the basic nature of MRI turbulence and the dissipation range. In the Plasma Couette Experiment (PCX), a hot, fast-flowing, steady-state plasma is created and confined in a largely magnetic field-free volume. Differential rotation is created via electrostatic stirring at inner and outer boundaries of a cylindrical plasma volume. To observe the MRI, flows must be adjusted to mimic Keplerian-like flows of astrophysical accretion disks, where angular velocity decreasing with radius, while still maintaining Rayleigh hydrodynamic stability with angular momentum increasing with radius.

This article will examine the effects of resistive and viscous dissipation, the Hall term, and plasma-neutral interactions pertinent to the onset of MRI in PCX. First, a description of PCX as it currently exists will be provided. The experiment has thus far operated with weakly-ionized ($\lesssim 1\%$) plasmas, and charge exchange collisions between ions and neutrals can have significant effects on the shape of flow profiles (Collins *et al.* 2012). Since the ion inertial length, $d_i \equiv c/\omega_{pi} \approx 1 - 3$ m, the Hall effect is expected to play an important role in PCX plasmas (Ebrahimi *et al.* 2011). A global stability analysis of the MRI that includes neutral drag and two-fluid effects will be presented. The results of this analysis will be shown to motivate major system upgrades to PCX. The specific benefits of these upgrades will be described in detail. Finally, a mechanism for driving flow with a body force across the whole plasma profile, which we simply call electrically driven flow (EDF), in PCX will be scribed along with a preliminary MRI stability analysis.

2. Description of Experiment

PCX consists of a roughly 1 m tall by 1 m diameter cylindrical vacuum chamber. The inner walls of the chamber are lined with toroidal rings of permanent magnets. This magnet geometry is shown below in Fig 6. The rings alternate polarity creating a multi-cusp magnetic field isolated to the edge of the vessel. The edge-localized field confines the plasma losses to a small cusp on the face of the magnets, while leaving the bulk volume unmagnetized. If desired, an external Helmholtz coil can produce nearly uniform axial magnetic fields in the chamber up to $B_0 \sim 50$ G.

A plasma discharge is created by biasing emissive thoriated tungsten cathodes to cold molybdenum anodes at up to 600V. The plasma is then heated with up to 6kW of electron cyclotron heating (ECH) to reach temperatures of $T_e \lesssim 10$ eV and densities of $n_e = 10^{10} - 10^{11} \text{ cm}^{-3}$. The hot cathodes also act to stir the plasma by drawing a current across the multi-cusp magnetic field at the edge. This $\mathbf{J} \times \mathbf{B}$ torque viscously couples inward to the unmagnetized bulk plasma. Due to the axisymmetric configuration of the magnets, particle drifts in the magnetized edge act to symmetrize the system, such that the toroidal location of the cathodes and anodes does not affect the flow drive (Katz *et al.* 2012). Flow can be driven at the inner boundary by a center core assembly consisting of 22 stacked magnet rings and up to 8 smaller thoriated tungsten cathodes biased with respect to cold anodes. This assembly can be entirely removed via a gate valve for maintenance of the cathodes.

Plasmas in PCX are routinely diagnosed with a swept or triple tip Langmuir probe for electron temperature and density, a cold cathode gauge for neutral pressure and Mach probes for flow velocity. In addition to these routine diagnostics, PCX has implemented Optical Emission Spectroscopy (OES) and a Fabry-Perot interferometer to measure electron and ion temperature. Both of these optical diagnostics are non-invasive, operating by simply sampling a single chord of emitted plasma light. The OES system takes a broadband spectrum of the plasma and uses line ratios to determine the electron temperature.

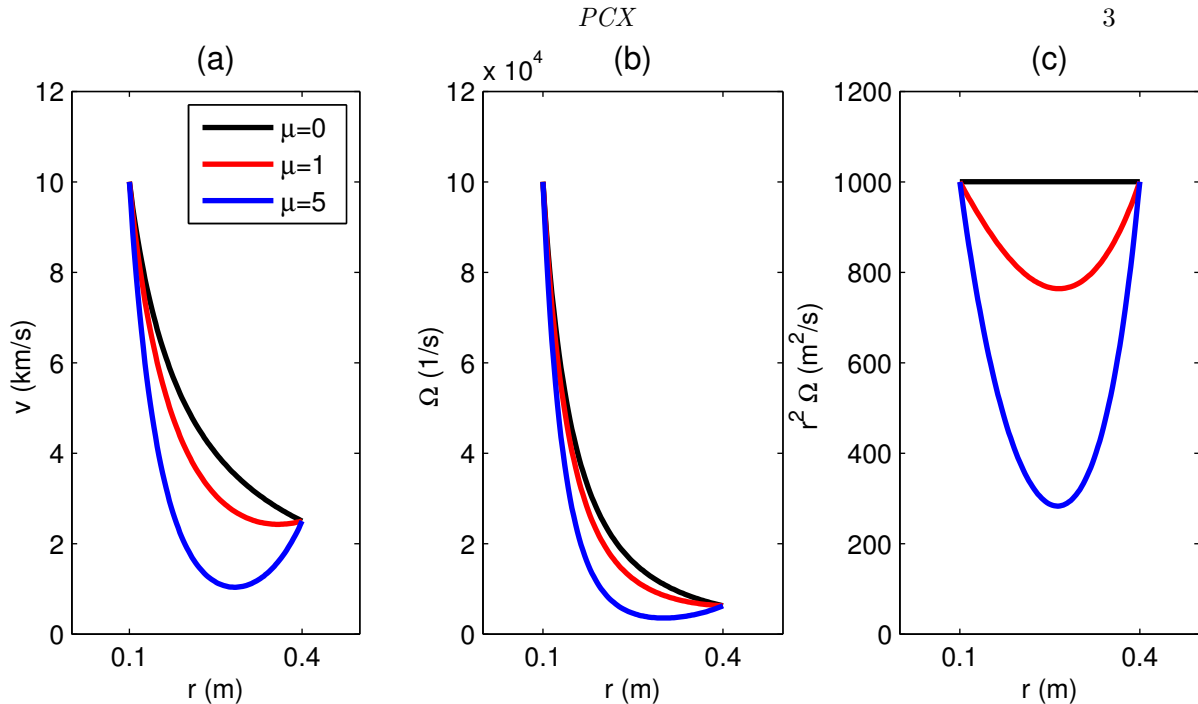


FIGURE 1. The (a) toroidal velocity, (b) angular frequency, and (c) angular momentum of synthetic modified Taylor Couette profiles with different $\mu \equiv L/L_\nu$ values.

OES temperature measurements in PCX agree within 15% of the routine Langmuir probe. The Fabry-Perot interferometer finely samples a small (< 1 nm) range of the emission spectrum centered at 468.6 nm in helium and 488 nm in argon. Ion emission lines at these wavelengths reflect the entire ion distribution function, such that the ion temperature and velocity can be deduced. In initial measurements of non-flowing argon plasmas, the ion temperature was determined to be $T_i = 0.2 - 1$ eV. This diagnostic is currently being refined for more accurate temperature and velocity measurements.

3. Taylor-Couette Flow (TCF) Profiles with Ion-Neutral Drag

TCF profiles of up to 12 km/s on the outer boundary and 3.75 km/s on the inner have been driven in helium PCX plasmas (Collins *et al.* 2014). These flows have areas of decreasing angular frequency as required by the ideal MRI criteria. They also have increasing angular momentum, thus meet the Rayleigh criterion for hydrodynamic stability. At PCX plasma parameters, these flows correspond to a magnetic Reynolds number of $Re \approx 26$ (using the outer boundary velocity) and a magnetic Prandtl number of $Pm \approx 2.5$.

In weakly-ionized plasmas, it has been shown (Collins *et al.* 2012) that charge exchange collisions between neutrals and ions imposes a drag force that affects the equilibrium (steady-state) velocity profiles. These profiles are a departure from ideal TCF, yet still have a simple Bessel function form:

$$V_\phi(r) = A\mathcal{I}_1(r/L_\nu) + BK_1(r/L_\nu) \quad (3.1)$$

where the constants A and B depend on the outer and inner boundary locations and the

velocities applied, $L_\nu^2 \equiv \tau_{i0}\nu$ is the momentum diffusion length, $\tau_{i0} = (n_0 \langle \sigma_{cx} v \rangle)^{-1}$ is the ion-neutral collision time, σ_{cx} is the ion-neutral charge exchange cross section, and ν is the kinematic viscosity due to ion-ion collisions. The momentum diffusion length parametrizes the balance between the viscous momentum diffusion and the neutral drag. When $L_\nu \ll r_2 - r_1$, the neutral drag dominates the viscous diffusion, rotation is confined to inner and outer edges of the plasma and the average velocity across the profile drops. In the opposite limit $L_\nu \gg r_2 - r_1$, the velocity profile becomes the ideal Taylor-Couette profile. With finite neutral drag, this effect has large qualitative effects on the velocity profile, which in turn greatly affect the stability of this modified TCF. Fig. 1 highlights the effect of neutral collisions on TCF profiles of toroidal velocity, angular frequency and angular momentum.

4. Global Stability Analysis

In order to capture two-fluid and neutral collision effects, an incompressible dissipative Hall MHD model with neutral-ion collisions is used for stability analysis. The governing equations are:

$$\frac{\partial \mathbf{V}}{\partial t} = -(\mathbf{V} \cdot \nabla) \mathbf{V} - \nabla \frac{P}{\rho} + \frac{1}{\mu_0 \rho} (\nabla \times \mathbf{B}) \times \mathbf{B} + \nu \nabla^2 \mathbf{V} - \frac{1}{\tau_{i0}} \mathbf{V} \quad (4.1)$$

$$\nabla \cdot \mathbf{V} = 0 \quad (4.2)$$

$$\frac{\partial \mathbf{B}}{\partial t} = \nabla \times \left[\mathbf{V} \times \mathbf{B} - \frac{1}{\mu_0 n e} (\nabla \times \mathbf{B}) \times \mathbf{B} \right] + \eta \nabla^2 \mathbf{B} \quad (4.3)$$

$$\nabla \cdot \mathbf{B} = 0 \quad (4.4)$$

where P is the scalar pressure, ρ is the mass density and η is the magnetic diffusivity (in m^2/s). In these equations, plasma parameters n_e , ρ , τ_{i0} , ν and η are assumed to be constant and uniform throughout the volume. The equilibrium modified TCF profile (Eq. 3.1) results from the steady-state balance between the last two terms in Eq. (4.1). In order to study linear stability, these equations are cast in terms of non-dimensional parameters and linearized near the equilibrium state: $\mathbf{V}_{eq} = V_\phi(r) \mathbf{e}_\phi$ and $\mathbf{B}_{eq} = B_0 \mathbf{e}_z$. The characteristic length is $L = H/2$, where H is the height of the plasma volume. Magnetic field strength and flow velocity are defined in terms of characteristic values: $\mathbf{B} = B_0 \mathbf{b}$ and $\mathbf{V} = V_0 \mathbf{v}$. The dimensionless equations are

$$\gamma \mathbf{v} = -(\mathbf{v}_{eq} \cdot \nabla) \mathbf{v} - (\mathbf{v} \cdot \nabla) \mathbf{v}_{eq} - \nabla p + \frac{1}{M_A^2} (\nabla \times \mathbf{b}) \times \mathbf{b}_{eq} + \frac{1}{Re} (\nabla^2 - \mu^2) \mathbf{v} \quad (4.5)$$

$$\gamma \mathbf{b} = \nabla \times \left[\mathbf{v}_{eq} \times \mathbf{b} + \mathbf{v} \times \mathbf{b}_{eq} - \frac{\delta_i}{M_A} (\nabla \times \mathbf{b}) \times \mathbf{b}_{eq} \right] + \frac{1}{Rm} \nabla^2 \mathbf{b} \quad (4.6)$$

where γ is the increment in units of V_0/L and $P \rightarrow \rho V_0^2 p$. The dimensionless parameters that enter these equations are: the fluid Reynolds number, $Re \equiv V_0 L / \nu$; the magnetic Reynolds number, $Rm \equiv V_0 L / \eta$; the Alfvén Mach number, $M_A \equiv V_0 / V_A \equiv V_0 \sqrt{\mu_0 \rho} / B_0$; the normalized ion inertial length for the Hall effect, $\delta_i \equiv d_i / L \equiv c / L \omega_{pi}$; and the normalized momentum diffusion length for the neutral collision effect, $\mu \equiv L / L_\nu \equiv L / \sqrt{\tau_{i0} \nu}$. These equations are then solved for axisymmetric modes using a standard finite difference method assuming no-slip, conducting side walls and periodicity in the axial direction.

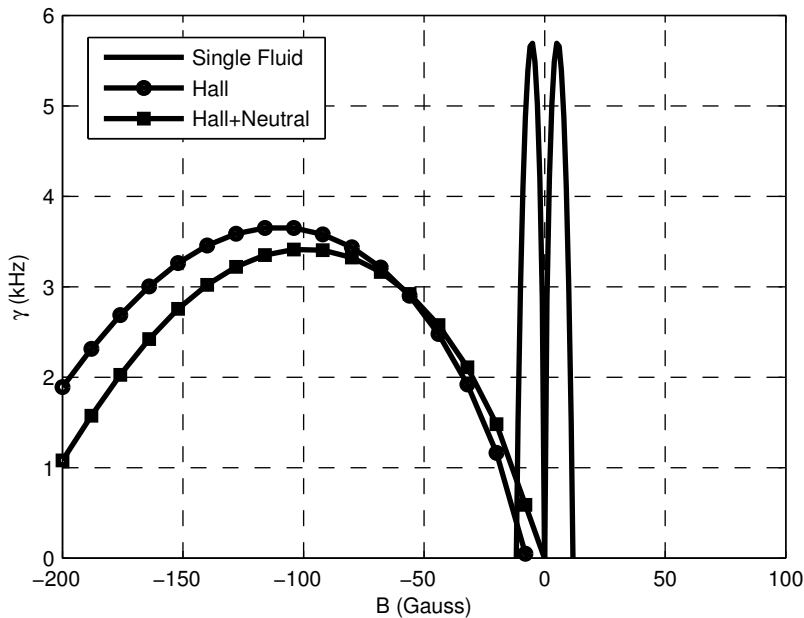


FIGURE 2. A comparison of the Hall and neutral collision effects on MRI Stability. For this case, $n = 10^{11} \text{ cm}^{-3}$ and $P_0 = 10^{-5} \text{ torr}$.

5. Results of Stability Analysis

Unless otherwise noted, all the analysis in this section is done assuming a singly ionized ($Z = 1$ and $n_e = n_i \equiv n$) helium plasma with $T_e = 12 \text{ eV}$ and $T_i = 0.4 \text{ eV}$. Fixing the temperatures allows viscosity to vary with density only and resistivity, η , to be mostly fixed (there is a weak density dependence). The dimensions of this system are $r_{inner} = 0.1 \text{ m}$, $r_{outer} = 0.4 \text{ m}$, and $H = 0.75 \text{ m}$, where the height determines the axial wave-number $k_z = \pi/L$. Finally, the inner and outer velocities are chosen to be the marginally stable ideal MRI case where $v_{inner} = \frac{r_{outer}}{r_{inner}} v_{outer}$. With no neutral drag, this gives a $v_\phi \propto \frac{1}{r}$ profile which satisfies the ideal MRI condition, $\partial\Omega^2/\partial \ln r < 0$, and the Rayleigh stability criterion, $\partial(r\Omega^2)/\partial r > 0$. For this analysis an inner velocity of $v_{inner} = 10 \text{ km/s}$ was chosen, which gives $v_{outer} = 2.5 \text{ km/s}$.

Figure 2 highlights the effects of the Hall and neutral collision terms on the MRI stability. This plot was produced at a density of $n = 10^{11} \text{ cm}^{-3}$ and a neutral pressure of $P_0 = 10^{-5} \text{ torr}$ ($n_0 \sim 3.2 \times 10^{11} \text{ cm}^{-3}$ assuming room temperature neutrals). For the ideal case, both the Hall and neutral collision effects are removed, leaving growth rates that are insensitive to the direction of B_0 . When the Hall term is included, positive growth rates are only found when the applied magnetic field is antiparallel to axis of rotation. Linear Hall-MHD global computations have been performed in the past by Ebrahimi *et al.* (2011) that show the same antiparallel requirement. These studies found, that in fully-ionized helium at relatively high densities, 6.5 km/s Keplerian flow profiles can excite the MRI with $n = 2 \times 10^{12} \text{ cm}^{-3}$, $T_e = 8 \text{ eV}$, and $T_i = 1.5 \text{ eV}$. Finally, if the neutral collision term is included, the growth rate is slightly reduced and the magnetic field at the peak growth rate is smaller in magnitude. These reductions are caused primarily by the lower average velocity, or Re , across the profile due to neutral drag.

By fixing, T_e , T_i , v_{inner} , v_{outer} and the dimensions of the system, the only parameters

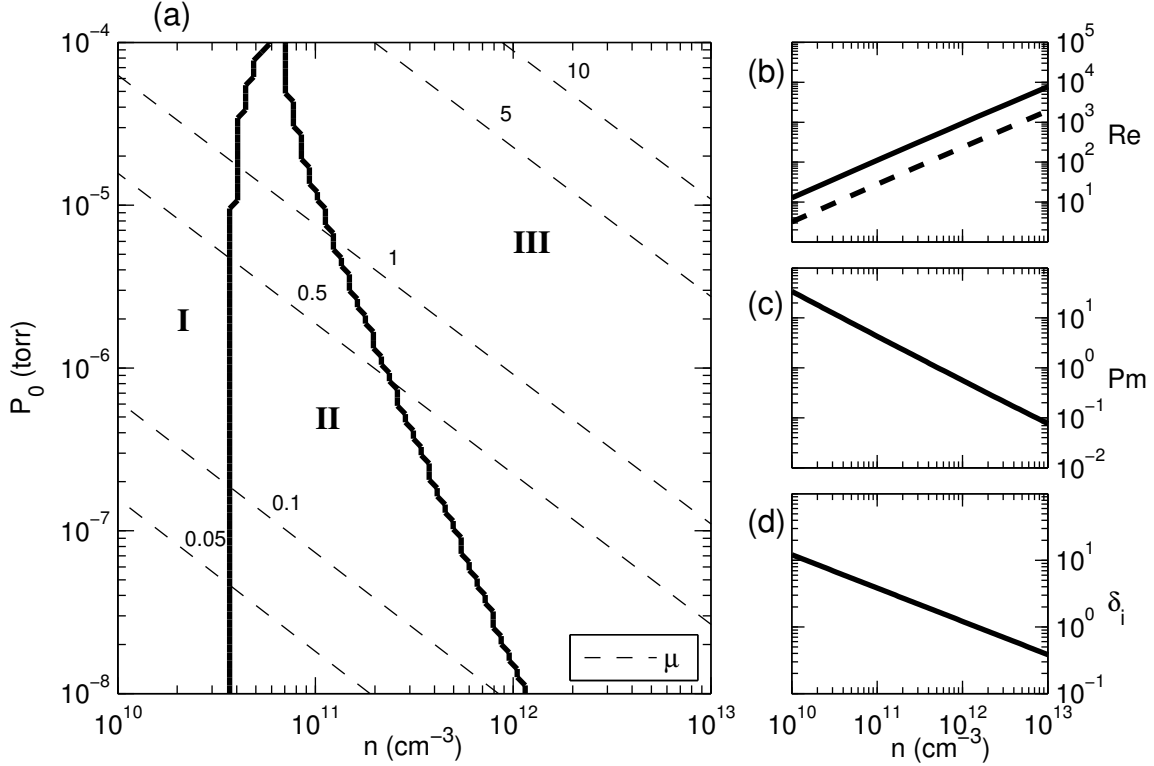


FIGURE 3. (a) Stability curves as functions of n and P_0 . For each n and P_0 the maximum growth rate in the range $B = -300$ to 100 Gauss is used to determine stability. Region I is stable. Region II is hydrodynamically stable, but unstable to the MRI. Region III is hydrodynamically and MRI unstable. Contours of μ are also plotted. On the right, the density dependence of (b) Re for both v_{inner} (solid) and v_{outer} (dashed), (c) $Pm \equiv Rm/Re$, and (d) δ_i are plotted.

left to vary are the plasma density, n ; the neutral pressure, P_0 ; and the magnetic field B_0 . With these three variables, we can manipulate all the dimensionless parameters given in the previous section.

$$\delta_i \propto n^{-1/2} \quad (5.1)$$

$$\mu \propto (nP_0 \ln \Lambda_{ii})^{1/2} \quad (5.2)$$

$$M_A \propto n^{1/2} B^{-1} \quad (5.3)$$

$$Re \propto n \log \Lambda_{ii} \quad (5.4)$$

$$Pm \propto (n \log \Lambda_{ii} \log \Lambda_{ei})^{-1} \quad (5.5)$$

where $\log \Lambda_{ii}$ and $\log \Lambda_{ei}$ are the weakly density dependent coulomb logarithms for ion-ion and electron-ion collisions, respectively. Figure 3a shows the instability regions as functions of n and P_0 . Region II represents the region where a MRI experiment would operate. Here, flowing plasmas are hydrodynamically stable, but an applied axial magnetic field sets off the MRI. It is clear that to ensure that an experiment is in region II with these fixed temperatures and flow velocities, the neutral pressure must be as low as possible and the density must be $n \sim 0.5 - 5 \times 10^{11} \text{ cm}^{-3}$. At higher neutral pressures and higher densities, μ can become of order unity, at which point the shear in the velocity profile caused by neutral drag is great enough to trigger hydrodynamic instabilities

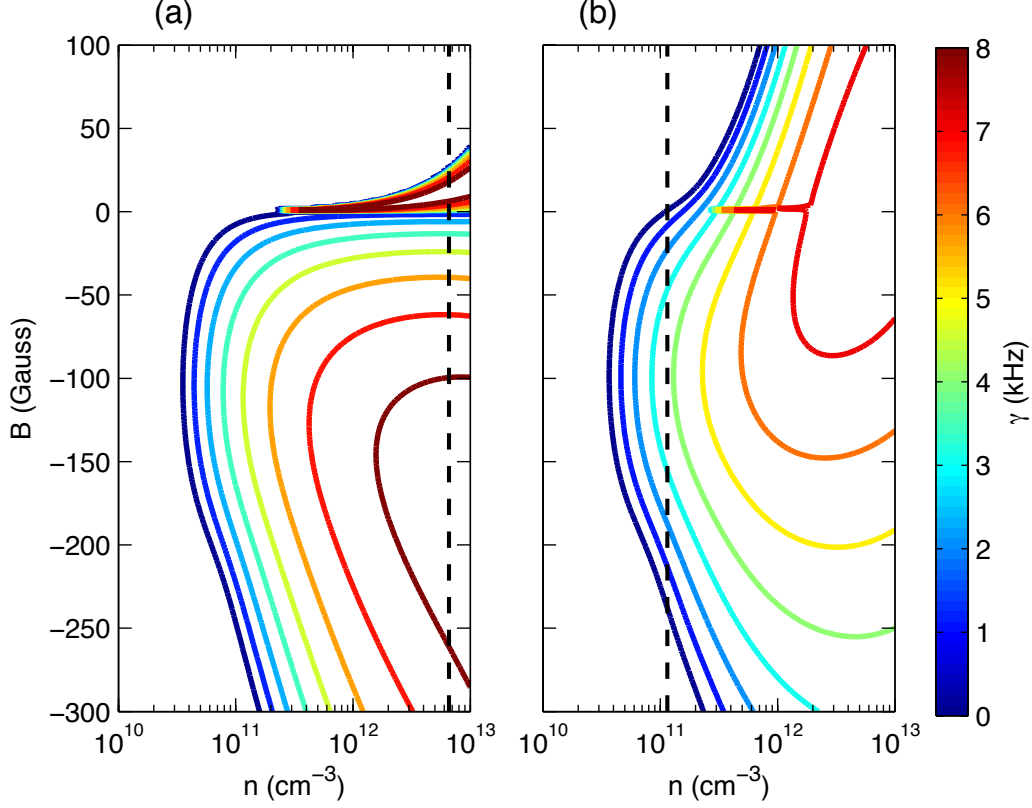


FIGURE 4. Contours of γ as a function of density and applied magnetic field for the case with no neutrals (a) and (b) the case with $P_0 = 10^{-5}$ torr. The dashed vertical line represents the density at these neutral pressures above which the flow becomes hydrodynamically unstable.

(region III). The MRI threshold appears to be mainly set by the density. For densities less than approximately $4 \times 10^{10} \text{ cm}^{-3}$, the viscosity is large enough to damp out the MRI. Currently on PCX, plasmas typically have densities $n_e = 2 - 6 \times 10^{10} \text{ cm}^{-3}$ and neutral pressures of about $P_0 = 1 \times 10^{-4}$ torr. These parameters put PCX in region I on this phase space diagram, where this flow is stable.

For fixed neutral pressures, Fig. 4 shows the effect of the Hall term on the MRI stability. At lower densities, where the Hall effect plays the largest role, positive MRI growth rates occur only for negative values of B_0 . This corresponds to the requirement that the flow be antiparallel to the magnetic field. As the density increases and the Hall effect weakens some positive growth rates appear for positive values of B_0 . When neutral collisions are included, the asymmetry from the Hall effect does persist until the flow becomes hydrodynamically unstable.

By scanning the velocity of the inner boundary at a fixed density and neutral pressure, a critical fluid Reynolds number can be found for MRI. Fig. 5 shows that for $n = 10^{11} \text{ cm}^{-3}$ and $P_0 = 10^{-5}$ torr, this critical Re is approximately 60 with a required magnetic field of about 25 Gauss. As the velocity increases, the peak magnetic field increases as well since $M_A \equiv V/V_A$ sets the MRI threshold for B_0 . At $Re \approx 180$, the flow becomes hydrodynamically unstable. According to Fig. 3, lower neutral pressures raise the critical Re for hydrodynamic instability.

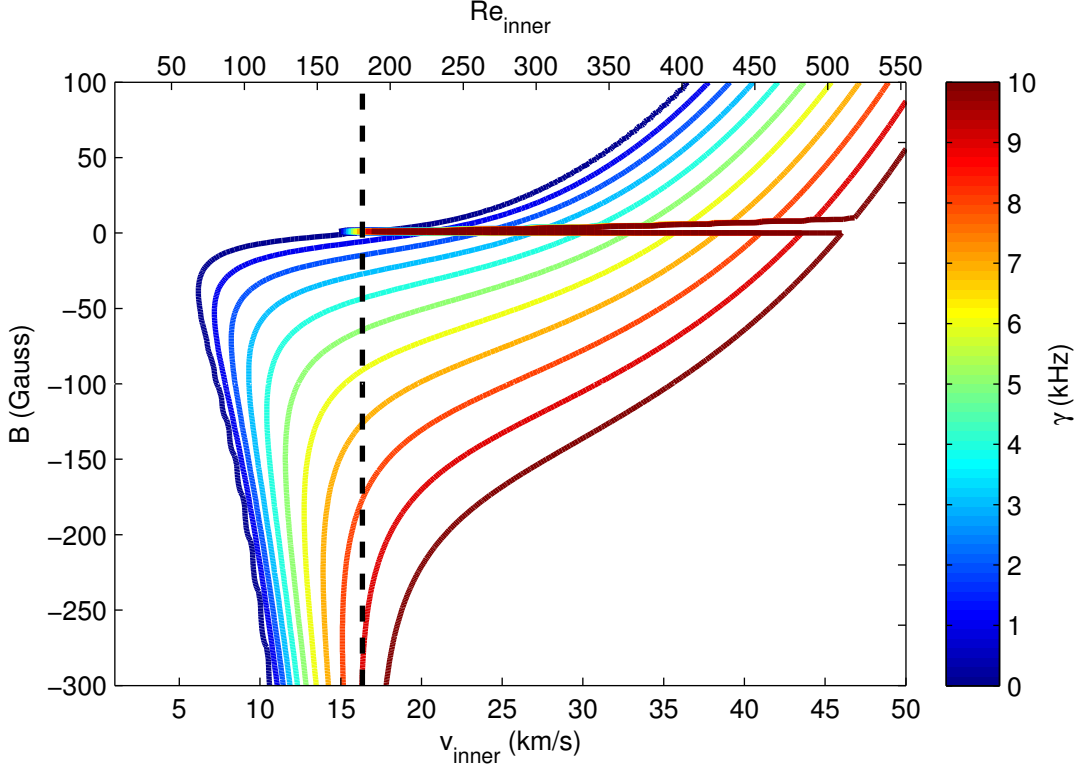


FIGURE 5. Contours of γ as a function of v_{inner} and applied magnetic field with density $n = 10^{11} \text{ cm}^{-3}$ and neutral pressure $P_0 = 10^{-5} \text{ torr}$.

6. Conclusions from Stability Study of Taylor-Couette Flow

From the stability analysis above, raising Re while keeping μ small is the key to reaching the MRI in PCX. One can raise Re by increasing the flow velocity or decreasing the viscosity, however this is a tradeoff between viscosity acting to transport momentum across the profile but also damping out any perturbations. At high viscosities, higher flow velocities are required to excite the MRI.

6.1. Flow Velocity Limits

Experimental evidence in PCX suggests that, at low ionization fractions, flow velocities are limited. Alfvén’s critical ionization theory (Alfvén 1954) predicts that when a flowing plasma is partially ionized, a critical ionization velocity (CIV) is set when the kinetic energy equals the ionization potential of the gas, U_i .

$$V_{CIV} = \sqrt{\frac{2eU_i}{m_i}} \quad (6.1)$$

Within a factor less than one, this simple theory has held up amazingly well over a large array of experiments (Brenning 1992; Lai 2001). In PCX, the highest flow velocities achieved in xenon, argon, neon and helium show that $V_{max} \sim V_{CIV}/3$.

Velocities at the inner boundary are also practically limited by current center core assembly design. The small tungsten cathodes have a relatively high failure rate compared

to the larger outer cathodes. At high biases, catastrophic arcs frequently destroy the inner cathodes. In order to reach higher inner boundary velocities (currently the maximum in helium is $v_{inner} \approx 3.75$ km/s), a more robust cathode design is required. A larger inner radius might also be used since, for a smaller gap, lower inner velocities are required to reach the same shear.

6.2. Density and Neutral Pressure Limits

If the velocity is limited, another way to increase Re is to increase the density, which decreases the viscosity at a fixed ion temperature and magnetic field strength. The density in PCX can be increased by increasing the pre-discharge fill pressure, however this leads to even lower ionization fractions. In order to raise the density without lowering the ionization fraction, better plasma confinement is needed.

The plasma confinement in a multi-cusp device is defined by particle and power balance equations. Since the bulk unmagnetized center of the plasma is very isotropic, gradients in temperature and density do not exist and a simple zero-dimensional boundary model of confinement can be used. The particle balance equation is defined by balancing the volumetric ionization rate with the boundary flux:

$$\langle \sigma_{iz} v_e \rangle n_e n_0 \mathbb{V} = 0.5 n_e c_s A_l \quad (6.2)$$

where σ_{iz} is the ionization cross section, \mathbb{V} is the plasma volume, c_s is the plasma sound speed, and A_l is the loss area. From particle balance alone, it is clear that increasing the ratio \mathbb{V}/A_l will result in lower n_0 for a given temperature. In order to see the effect of increasing \mathbb{V}/A_l on plasma density, power balance must also be considered.

A zero-dimensional particle and power balance model has been implemented on the Madison Plasma Dynamo Experiment (MPDX) to predict plasma parameters (density, temperature), given laboratory parameters (input power, fill pressure). This code has been benchmarked with real MPDX data (Cooper *et al.* 2014) and can be applied to other multi-cusp confinement devices, like PCX. Preliminary results from this code show that for a given power and fill pressure, the density and ionization fraction increase with a larger \mathbb{V}/A_l ratio. Also, predictably, plasma density and ionization fraction both increase with increased power. Clearly, to lower the neutral pressure and raise the density in PCX, a larger \mathbb{V}/A_l ratio and more power are required.

7. Proposed System Upgrades

An upgrade to the confinement and heating systems for PCX is underway. The goals are to improve confinement by increasing \mathbb{V}/A_l , input more power, and to improve the temperature tolerances of PCX in order to accommodate longer and higher power discharges. These upgrades, referred to as PCX-U from here on, constitute a major change for PCX that collectively aim to push the experiment into MRI relevant parameter regimes.

The largest portion of the PCX upgrade consists of an entirely new magnet assembly. Approximately 1900 samarium cobalt (SmCo) magnets, like those used in MPDX (Cooper *et al.* 2014), will replace the current array of ceramic magnets. These magnets, while still being fairly inexpensive, have a much higher field strength and temperature tolerance. For the sizes and grade proposed, the field will be approximately 4 kG at the face of the magnets (the ceramic magnets are 1 kG) and the maximum operating temperature will be nearly 300° C.

The new magnets themselves are a large improvement over the current system. Currently, the length of PCX discharges is mostly limited by the temperature that the magnets reach, which is ideally kept below about 60°C. With a higher temperature tolerance,

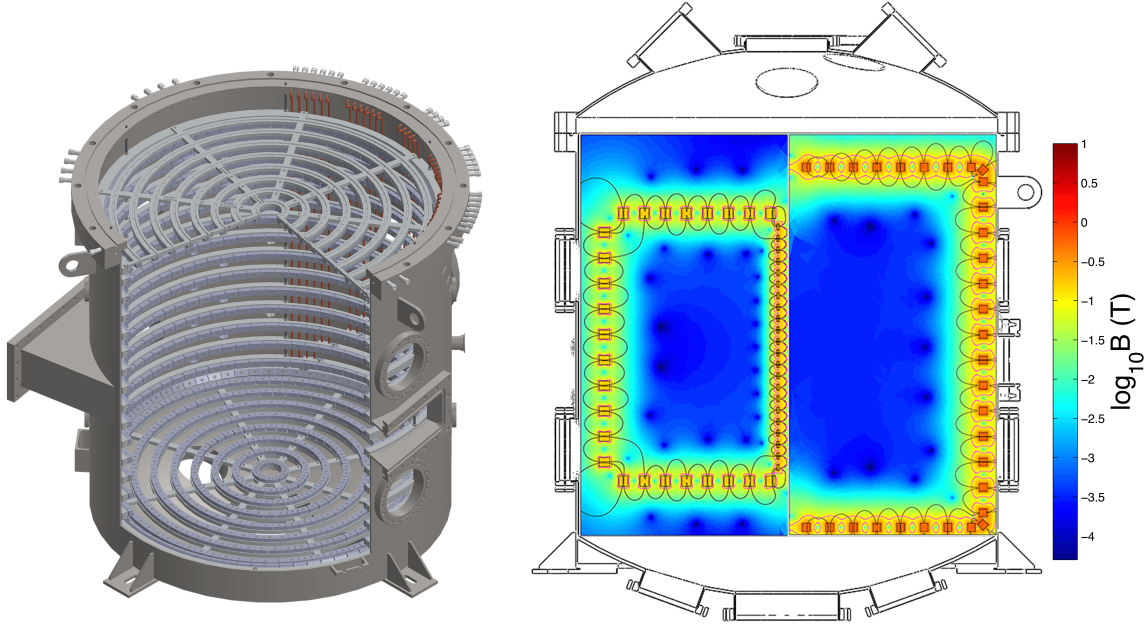


FIGURE 6. Left: A design image of the proposed new magnet assembly on PCX-U. Right: A comparison of the current PCX magnet geometry (left) and the proposed geometry (right). These plots show the magnitude of the magnetic field on a scale from Earth’s field to 1 T. The pink contour is the 875G ECRH resonance.

the SmCo magnets will allow for longer discharges. In turn, good vacuum pumping and longer discharges will allow for more neutrals to be removed. Additionally, the four-fold increase in magnetic field strength reduces the cusp loss width. The cusp width can be estimated as $w = 4\sqrt{\rho_i\rho_e} \propto B^{-1}$, where ρ_i and ρ_e are the ion and electron gyroradii, respectively (Hershkowitz *et al.* 1975). This smaller width represents an increase in the ∇/A_l ratio.

The left image of Figure 6 shows a design image of the new magnet assembly. Approximately 1000 magnets will be bolted to 14 individually water cooled aluminum rings equal spaced in the axial direction. At the top and bottom of the chamber, 8 concentric rings attached by spokes carrying water cooling will support an additional 350 magnets each. Finally, two rings pitched at 45° will be supported in the corners between the top and bottom rings and the side rings. These angled rings serve to strengthen the field at the corners where the current assembly suffers from the most magnet heating. The whole assembly is supported by 6 rods attached to a top flange which doubles as the water cooling vacuum feedthrough. The inner three rings on the top and bottom assemblies may be removed in order to place center cathode assemblies of up to 16in in diameter into PCX-U.

On the right in Figure 6, a side by side comparison of the current and new magnet assemblies highlights the roughly 150% increase in plasma volume. Due to the extra rings of magnets, the cusp length of the new assembly is roughly 130% longer, but the stronger magnets make the cusp width smaller, so the ∇/A_l ratio is about 4.5 times larger on PCX-U. This is a significant improvement in confinement, which will allow higher plasma densities and temperatures.

In addition to the new magnet assembly, PCX-U includes a new 6kW magnetron for increased plasma heating, doubling the existing available microwave power. At densities

above, $n = 7.4 \times 10^{10} \text{ cm}^{-3}$, PCX plasmas are above the O-mode cutoff for 2.45 GHz, yet it has been observed that microwave power still heats the plasma via surface wave discharges (Collins *et al.* 2014). To reach the densities $n \sim 10^{11} \text{ cm}^{-3}$, PCX will need to operate in this overdense mode. Additionally, the stronger field on the magnets places the 875 G ECH resonance further into the plasma volume, thus the surface wave discharge will have a larger volume to fill. This extra power will be managed by the high temperature tolerance of the SmCo magnets.

8. Electrically Driven Flow

Achieving MRI relevant flows is another challenge for PCX-U. Reaching high flow speeds on the inner boundary has proven to be difficult based on the space and power constraints of the center column assembly. Electrically driven flow (EDF) offers an alternative to Taylor-Couette flow that does not require inner boundary string electrodes.

In EDF, a radial electrical current flowing through uniform axial magnetic field creates $\mathbf{J} \times \mathbf{B}$ torque, which acts as the azimuthal body force. The resulting azimuthal velocity in EDF for the bulk of the fluid has $v_\phi \propto 1/r$ profile. As opposed to TCF, the EDF profile shape is unchanged for different magnitudes of total radial current. This removes the freedom of creating an arbitrary azimuthal velocity profile, but guarantees a profile that is unstable with respect to the MRI.

In PCX-U, the Helmholtz coil supplies an axial magnetic field while a single cathode or anode can be placed in the center of the vessel and biased to electrodes on the outer wall to draw the cross field current. The simplicity of this system is experimentally very attractive because a center core assembly is not required.

In order to increase the current output of PCX cathodes, lanthanum hexaboride (LaB6) will be used instead of thoriated tungsten for Dean flow. This material has an extremely low work function and, when heated, is a superb electron emitter. LaB6 cathodes used in MPDX can typically draw tens of amperes of current, which represents an order of magnitude increase over the tungsten PCX cathodes (Cooper *et al.* 2014).

8.1. Equilibrium

Analysis of EDF flow in relation to MRI has been presented in various parameter regimes (Noguchi & Pariev 2003; Khalzov *et al.* 2006, 2010) using dissipative single-fluid MHD. In this analysis, Hall and neutral collision terms are included to reflect the regime of weakly ionized, sparse plasmas. As an initial step, the axisymmetric equilibrium state ($\partial/\partial t \rightarrow 0$) described by system of equations (4.1)-(4.4) is found assuming perfectly conducting inner and outer cylinders and insulating top and bottom ends and no-slip boundary conditions for velocity at the walls. The system is discretized in two-dimensional r - z domain and solved by an iterative method outlined in (Khalzov *et al.* 2010).

Several key features are present in the equilibrium EDF profiles. First, there are thin Hartmann layers near the top and bottom ends, which scale like $1/Ha$, and parallel layers near side walls, which scale like $1/Ha^{1/2}$, where $Ha \equiv V_A L / \sqrt{\nu \eta} = \sqrt{Re Rm} / M_A$ is the Hartmann number (Khalzov *et al.* 2010). With exception of these boundary layers (which are narrow if $Ha \gg 1$), the bulk of the plasma rotates with azimuthal velocity $v_\phi \propto 1/r$.

Second, since the driving $\mathbf{J} \times \mathbf{B}$ force for EDF is a body force applied across the whole profile, the neutral drag acts only to uniformly lower the magnitude of the profile. Increased neutral density no longer results in a qualitative change to the shape of the profile like it does for TCF. This simplifies the effects of ion-neutral collisions in the following stability analysis. Similarly, the Hall term acts to uniformly increase the magnitude of the profile (at fixed total radial current). This is illustrated in Fig. 7.

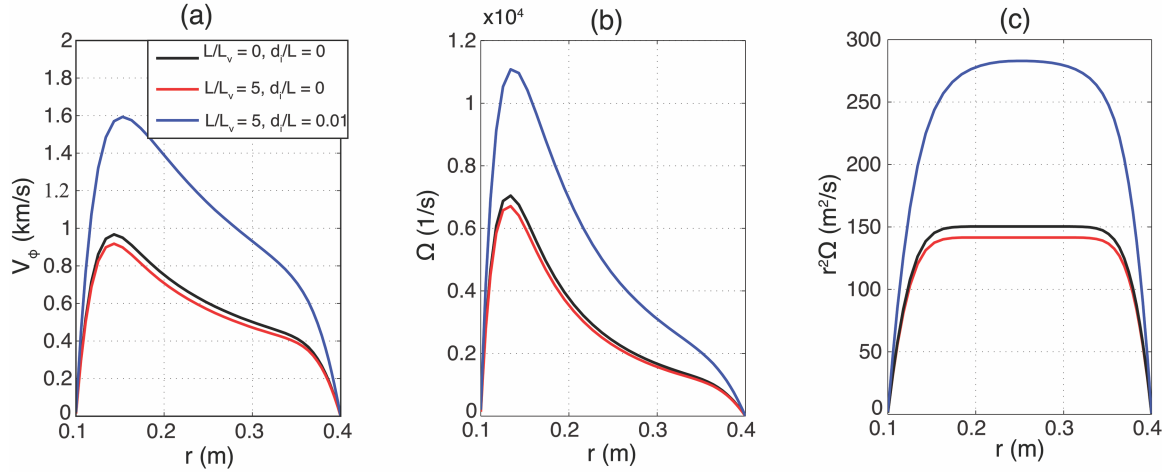


FIGURE 7. The radial profiles of (a) azimuthal velocity, (b) angular frequency, and (c) angular momentum of electrically driven flow showing effects of neutral drag and Hall term. Calculations are done for helium plasma with density $n = 10^{12} \text{ cm}^{-3}$, electron temperature $T_e = 12 \text{ eV}$, ion temperature $T_i = 0.4 \text{ eV}$, total radial current $I_0 = 100 \text{ A}$ and axial magnetic field $B_0 = 10 \text{ Gs}$ (corresponding to $Re = 18$, $Rm = 10$, $Ha = 385$).

Third, as shown in (Khalzov *et al.* 2010), the magnitude of induced magnetic field scales as Rm/Ha , while the magnitude of poloidal flow scales as Re/Ha^2 . At large Hartmann numbers these quantities become small, therefore they can be neglected in the stability analysis. For the stability analysis, the presence of the boundary layers is also neglected. Additionally it is assumed that the plasma rotates in the uniform axial field B_0 with azimuthal velocity $v_\phi = A/r$, where amplitude A is determined from the equilibrium solver (it depends on total current I_0 , neutral drag and Hall effect).

Note, that the neglected boundary layers may lead to some additional parasitic instabilities, especially the layer near the outer wall, where the angular momentum is decreasing (and, therefore, hydrodynamically unstable). This problem can be overcome experimentally by adjusting the positions of the near-wall electrodes in such a way, that in addition to bulk forcing they produce a local drive in the cusp region (like in the TCF) to equalize boundary and bulk angular momenta.

8.2. Stability

The following results are obtained for singly ionized helium plasma with density $n = 10^{12} \text{ cm}^{-3}$, electron temperature $T_e = 12 \text{ eV}$, ion temperature $T_i = 0.4 \text{ eV}$, neutral pressure $P_0 = 10^{-5} \text{ torr}$ in the cylinder with sizes $R_1 = 0.1 \text{ m}$, $R_2 = 0.4 \text{ m}$, $H = 0.75 \text{ m}$.

The stability of the equilibrium flow with $v_\phi = A/r$ in an uniform axial field B_0 is studied by solving the eigenvalue problem resulting from linearizing system (4.5)-(4.6). The MRI boundary as a function of external field B_0 and total current I_0 is given in Fig. 8. The familiar Hall effect is also present in the electrically driven flow where the axis of the flow must be antiparallel to the axial magnetic field to get positive MRI growth rates. This means that current must flow from the inner to outer boundary of the plasma. Experimentally, this means that cathodes at the outer edge must be negatively biased with respect to an anode close to ground placed in the center.

Fig. 8 also demonstrates that several modes with different k_z will be excited almost simultaneously when the MRI threshold is reached. Such multi-mode instability may

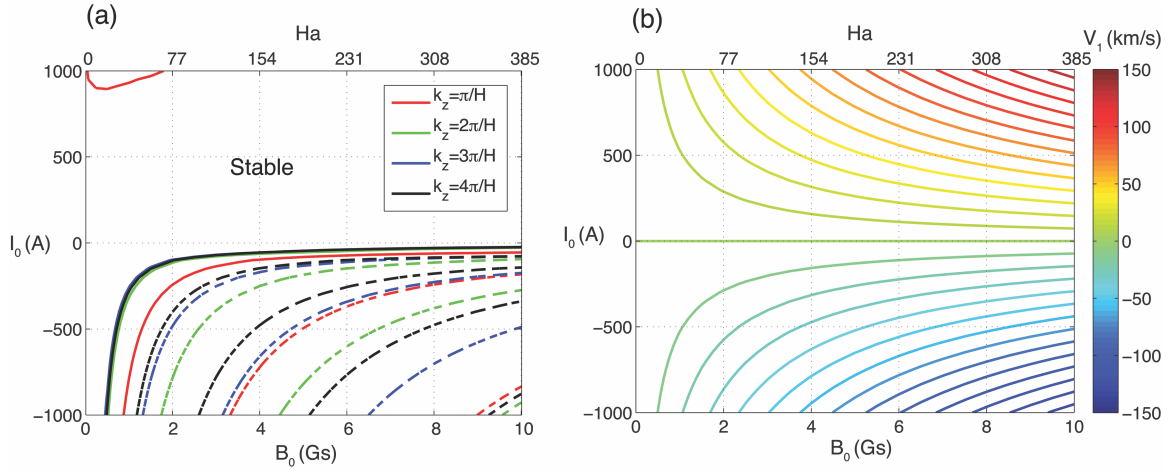


FIGURE 8. (a) MRI regions in electrically driven flow for modes with different axial wave-numbers k_z . Dashed lines of the same color denote stability boundaries for modes with the same k_z but different radial mode numbers. (b) Azimuthal velocity at the inner wall. Plasma parameters are listed in the text. Negative sign of I_0 corresponds to current flowing from the inner to outer wall.

lead to fast development of turbulence, which is another intriguing objective for the proposed plasma MRI experiment.

9. Summary

The prospects for observing the MRI in PCX are good. In this paper, the effects of plasma dynamics pertinent to the PCX regime on the MRI have been studied via a global stability analysis. From this study, an experimentally achievable regime has been found where the MRI should be excited. Experimental considerations have led to a currently undergoing upgrade to put PCX in this regime. Finally, so-called electrically driven flow is considered as an alternative to Taylor-Couette flow and shown to lead to the MRI with PCX-U parameters.

A global stability analysis for weakly-ionized, sparse plasmas has highlighted the combined effects of ion-neutral collisions and the Hall term on the MRI. As previously noted, the Hall term leads to a requirement that the seed magnetic field be antiparallel to the axis of rotation for positive MRI growth rates. Ion-neutral collisions effectively add a drag force to the momentum equation. This drag quantitatively changes the Taylor-Couette profile shape and leads to a small region in parameter space where flows are unstable to the MRI, while maintaining hydrodynamic stability.

Upgrades to PCX are motivated by the need to reduce the neutral drag force in order to avoid hydrodynamic instability at large Re . A new magnetic cusp assembly will provide better confinement quantified by a factor of 4.5 increase in the volume to loss area ratio. In addition to better confinement, upgrades will act to harden PCX for longer and higher power plasma discharges.

Finally, an experimental configuration for EDF provides an alternative to Taylor-Couette flow that is both experimentally attractive due to its simplicity and less susceptible to large adverse effects due to ion-neutral collisions. Due to the lack of a center core assembly, EDF can be realized in PCX with high power LaB6 cathodes capable of drawing tens of amps each. Additionally because EDF is driven by a body force, the

ion-neutral drag causes no qualitative changes in the $v_\phi \propto r^{-1}$ profile shape. Preliminary global stability analysis of EDF profiles shows that the MRI can be excited at experimentally achievable parameters.

This work was funded in part by National Science Foundation and the Center for Magnetic Self Organization in Laboratory and Astrophysical Plasmas.

REFERENCES

- ALFVÉN, H. 1954 *On the Origin of the Solar System*. New York: Oxford Univ. Press.
- BALBUS, S. & HAWLEY, J. 1991 A powerful local shear instability in weakly magnetized disks. *ApJ* **376**, 214–222.
- BALBUS, S. & HAWLEY, J. 1998 Instability, turbulence, and enhanced transport in accretion disks. *Rev. Mod. Phys.* **70**, 1–53.
- BALBUS, S. A. & TERQUEM, C. 2001 Linear analysis of the hall effect in protostellar disks. *ApJ* **552**, 235–247.
- BRENNING, N. 1992 Review of the civ phenomenon. *Space Science Reviews* **59** (3–4), 209–314.
- CHANDRASEKHAR, S. 1960 The stability of non-dissipative couette flow in hydromagnetics. *Proc. Natl. Acad. Sci.* **46**, 253–257.
- COLLINS, C., CLARK, M., COOPER, C. M., FLANAGAN, K., KHALZOV, I. V., NORBERG, M. D., SEIDLITZ, B., WALLACE, J. & FOREST, C. B. 2014 Taylor-couette flow of unmagnetized plasma. *Phys. Plasmas* **21** (042117).
- COLLINS, C., KATZ, N., WALLACE, J., JARA-ALMONTE, J., REESE, I., ZWEIBEL, E. & FOREST, C.B. 2012 Stirring unmagnetized plasma. *Phys. Rev. Lett.* **108** (115001).
- COOPER, C. M., WALLACE, J., BROOKHART, M., CLARK, M., COLLINS, C., DING, W. X., FLANAGAN, K., KHALZOV, I., LI, Y., MILHON, J., NORBERG, M., NONN, P., WEISBERG, D., WHYTE, D. G., ZWEIBEL, E. & FOREST, C. B. 2014 The madison plasma dynamo experiment: A facility for studying laboratory plasma astrophysics. *Phys. Plasmas* **21** (013505).
- EBRAHIMI, F., LEFEBVRE, B., FOREST, C.B. & BHATTACHARJEE, A. 2011 Global hall-mhd simulations of magnetorotational instability in a plasma couette flow experiment. *Phys. Plasmas* **18** (062904).
- HERSHKOWITZ, N., LEUNG, K. N. & ROMESSER, T. 1975 Plasma leakage through a low- β line cusp. *Phys. Rev. Lett.* **35** (277).
- KATZ, N., COLLINS, C., WALLACE, J., CLARK, M., WEISBERG, D., JARA-ALMONTE, J., REESE, I., WHAL, C. & FOREST, C.B. 2012 Magnetic bucket for rotating unmagnetized plasma. *Rev. Sci. Instr.* **83** (063502).
- KHALZOV, I. V., ILGISONIS, V. I., SMOLYAKOV, A. I. & VELIKHOV, E. P. 2006 Magnetorotational instability in electrically driven flow of liquid metal: Spectral analysis of global modes. *Phys. Fluids* **18** (12).
- KHALZOV, I. V., SMOLYAKOV, A. I. & ILGISONIS, V. I. 2010 Equilibrium magnetohydrodynamic flows of liquid metals in magnetorotational instability experiments. *J. Fluid Mech.* **644**, 257–280.
- LAI, S. 2001 A review of critical ionization velocity. *Reviews of Geophysics* **39** (4), 471–506.
- LONGARETTI, P. Y. & LESUR, G. 2010 Mri-driven turbulent transport: the role of dissipation, channel modes and their parasites. *A&A* **516** (A51).
- NOGUCHI, KOICHI & PARIIEV, VLADIMIR I. 2003 Magnetorotational instability in a couette flow of plasma. *AIP Conference Proceedings* **692** (1), 285–292.
- VELIKHOV, E. P. 1959 Stability of an ideally conducting liquid flowing between cylinders rotating in a magnetic field. *J. Exptl. Theoret. Phys.* **36**, 1398–1404.
- WARDLE, M. 1999 The balbus-hawley instability in weakly ionized disks. *Mon. Not. R. Astron. Soc.* **307**, 849–856.